

SOLVING STIFF PDES IN 1D, 2D AND 3D WITH EXPONENTIAL INTEGRATORS

HADRIEN MONTANELLI* AND NIALl BOOTLAND†

Abstract. Dozens of exponential integration formulas have been proposed for the high-accuracy solution of stiff PDEs such as the Korteweg-de Vries, Allen-Cahn, nonlinear Schrödinger and Gray-Scott equations. We report the results of extensive comparisons of such formulas in 1D, 2D and 3D, focusing on fourth and higher order methods and periodic problems. Our conclusion is that it is hard to do much better than one of the simplest of these formulas, the ETDRK4 scheme of Cox and Matthews [12].

Key words. Stiff PDEs, exponential integrators, Fourier spectral methods

AMS subject classifications. 65L04, 65L05, 65M20, 65M70

1. Introduction. We are interested in solving stiff PDEs of the form

$$u_t = \mathcal{S}(u) = \mathcal{L}u + \mathcal{N}(u), \quad u(0, X) = u_0(X), \quad (1.1)$$

where $u(t, X)$ is a function of time t and space X , \mathcal{L} is a linear differential operator on a domain in one, two or three space dimensions and \mathcal{N} is a nonlinear differential (or non-differential) operator of lower order on the same domain¹. In applications, PDEs of this kind typically arise when two or more different physical processes are combined, and many PDEs of interest in science and engineering take this form. For example, the Korteweg-de Vries equation $u_t = -u_{xxx} - uu_x$, the starting point of the study of nonlinear waves and solitons, couples third-order linear dispersion with first-order convection, and the Allen-Cahn equation $u_t = \epsilon u_{xx} + u - u^3$ couples second-order linear diffusion with a nondifferentiated cubic reaction term. Often a system of equations rather than a single scalar equation is involved, for example in the Gray-Scott and Schnakenberg equations, which involve two components coupled together. (The importance of coupling of nonequal diffusion constants in science was made famous by Alan Turing in the most highly-cited of all his papers [59].) Fourth-order terms also arise, for example in the Cahn-Hilliard equation, whose solutions describe structures of alloys, and in the Kuramoto-Sivashinsky equation, related to combustion problems among others, whose solutions are chaotic. Other examples of stiff PDEs include the viscous Burgers, Ginzburg-Landau, nonlinear Schrödinger and Swift-Hohenberg equations.

Solving all these PDEs by generic numerical methods can be highly challenging. This paper describes and compares specialized methods that take advantage of two special features of (1.1). The first is that in many applications boundary effects are not the scientific issue, so that it suffices to consider periodic domains. This allows us to discretize the spatial component of (1.1) with a Fourier spectral method on N points; equation (1.1) becomes a system of N ODEs,

$$\hat{u}' = \mathbf{S}(\hat{u}) = \mathbf{L}\hat{u} + \mathbf{N}(\hat{u}), \quad \hat{u}(0) = \hat{u}_0, \quad (1.2)$$

*Oxford University Mathematical Institute, Oxford OX2 6GG, UK. Supported by the European Research Council under the European Union's Seventh Framework Programme (FP7/2007–2013)/ERC grant agreement no. 291068. The views expressed in this article are not those of the ERC or the European Commission, and the European Union is not liable for any use that may be made of the information contained here.

†Oxford University Mathematical Institute, Oxford OX2 6GG, UK. This publication was based on work supported in part by award no. KUK-C1-013-04, made by King Abdullah University of Science and Technology (KAUST).

¹ X denotes a space variable in 1D, 2D or 3D. Throughout this paper, we will use the variables x in 1D, (x, y) in 2D and (x, y, z) in 3D.

where $\hat{u}(t)$ is a vector of N Fourier coefficients, and \mathbf{L} (a $N \times N$ matrix) and \mathbf{N} are the discretized versions of \mathcal{L} and \mathcal{N} . For example, in 1D on $[0, 2\pi]$ with $\mathcal{L}u = u_{xx}$ and an even number N of equispaced grid points $\{x_j = 2\pi j/N\}_{j=0}^{N-1}$, we look for a solution $u(t, x)$ of the form²

$$u(t, x) \approx \sum'_{k=-N/2}^{N/2} \hat{u}_k(t) e^{ikx} \quad (1.3)$$

with Fourier coefficients³

$$\hat{u}_k(t) = \frac{1}{N} \sum_{j=0}^{N-1} u(t, x_j) e^{-ikx_j}, \quad -\frac{N}{2} \leq k \leq \frac{N}{2} - 1, \quad \hat{u}_{N/2}(t) = \hat{u}_{-N/2}(t). \quad (1.4)$$

For this PDE, $\mathbf{L} = \mathbf{D}^{(2)}$ is the (diagonal) *second-order Fourier differentiation matrix* with entries $-k^2$, $-N/2 \leq k \leq N/2 - 1$; see [57] for more details about Fourier spectral methods and [61] for a review of trigonometric interpolation techniques. Some basic results about Fourier spectral methods and trigonometric interpolation can be found in Appendices A (1D) and B (2D and 3D).

The main issue with solving (1.2) numerically is stiffness, characterised by the need for an explicit method to use small time-steps, much smaller than the condition required by accuracy. (Note that stiffness is related to \mathbf{L} having large eigenvalues since stability of spectral methods for time-dependent PDEs requires that the eigenvalues of \mathbf{L} , scaled by the time-step, lie in the stability region of the time-stepping formula [57, Chapter 10].) When too many steps are required, this can result in an infeasibly long computation for the method.

The second special feature of (1.1) is that the higher-order terms of the equation are linear. Exponential integrators are a class of numerical methods for systems of ODEs which are aimed at taking advantage of this. The linear part \mathbf{L} , responsible for the stiffness, is integrated exactly using the matrix exponential while a numerical scheme is applied to \mathbf{N} .

According to the 2005 review of Minchev and Wright [39], the first exponential integrators were constructed in a paper by Certaine [10], published in 1960. Subsequently, however, Hochbruck and Ostermann [24] noted, in a comprehensive theoretical review of these schemes, that Hersch [21] had previously considered exponential integrators in 1958 in an effort to find schemes which are exact for linear problems with constant coefficients. The first use of the term *exponential integrator* was by Hochbruck, Lubich and Selhofer [22] in a seminal paper of 1998. The extensive use of these formulas for solving stiff PDEs seems to have been initiated by the papers by Cox and Matthews [12] and Kassam and Trefethen [29]. A striking unpublished paper by Kassam [28] shows how effective such methods can be also for PDEs in 2D and 3D. A software package for such computations called EXPINT was produced by Berland, Skaflestad and Wright [4].

One of the simplest exponential integrators, first derived by Pope in 1963 [42] and commonly known as the Exponential Time Differencing (ETD) Euler method, is given by⁴

$$\hat{u}_{n+1} = e^{h\mathbf{L}} \hat{u}_n + h\varphi_1(h\mathbf{L})\mathbf{N}(\hat{u}_n), \quad (1.5)$$

²The prime on the summation sign in (1.3) signifies that the terms $k = \pm N/2$ are halved.

³Note that, in practice, the coefficient $\hat{u}_{N/2}$ is not stored—the vector of Fourier coefficients is really $\hat{u}(t) = \{\hat{u}_k(t)\}$, with $-N/2 \leq k \leq N/2 - 1$.

⁴Throughout this paper, when introducing an exponential integrator such as (1.5), \hat{u}_n will mean $\hat{u}(t)$ at $t = t_n$.

where $h = t_{n+1} - t_n$ is the time-step and

$$\varphi_1(z) = \frac{e^z - 1}{z}. \quad (1.6)$$

As Minchev and Wright [39] point out, this method has been rediscovered from many different viewpoints and has been known by several other names. Pope introduced it by considering the linearized version of (1.2) on $[t_n, t_{n+1}]$,

$$\hat{u}' = \mathbf{S}(\hat{u}_n) + (\hat{u} - \hat{u}_n)\mathbf{S}_{\hat{u}}(\hat{u}_n), \quad \hat{u}(t_n) = \hat{u}_n, \quad (1.7)$$

with exact solution at $t_{n+1} = t_n + h$,

$$\hat{u}_{n+1} = \hat{u}_n + h\varphi_1(h\mathbf{S}_{\hat{u}}(\hat{u}_n))\mathbf{S}(\hat{u}_n). \quad (1.8)$$

Approximating $\mathbf{S}_{\hat{u}}(\hat{u}_n)$ by \mathbf{L} in (1.8) leads to (1.5). Note that (1.8) defines a time-stepping scheme too, known as the exponential Euler method. The problem with (1.8) is that the exact Jacobian $\mathbf{S}_{\hat{u}}$, and its value under the exponential-like function φ_1 , need to be computed at each time-step. This would involve a high computational cost, so typically one either does not compute φ_1 but rather an approximation, such as a Padé approximation, or else one uses an approximation to the Jacobian as opposed to the exact Jacobian. The former approach contains the Rosenbrock methods. There is a large literature on such methods, including the papers of Rosenbrock [45] and Hairer [18] and the books of Hairer and Wanner [19] and van der Houwen [60]. More recent papers include Hochbruck et al. [26] and Luan and Ostermann [36]. The latter approach is what Pope did to derive (1.5) and is what we shall consider in this paper.

As we just described, exponential integrators are characterised by the use of exponential and related functions of the matrix \mathbf{L} . Standard methods for computing the matrix exponential include Krylov subspace methods and the scaling and squaring method together with a truncated Taylor series approximation to the exponential [1]. There is recent work which shows that exponential integrators together with Krylov methods are competitive, for instance see Tokman and Loffeld [34, 53]. In our case we consider periodic problems and, using Fourier spectral methods, the matrices \mathbf{L} are diagonal, so we can work with scalars as opposed to matrices.

We compare in this paper thirty exponential integrators of fourth and higher order on fourteen model problems in 1D, 2D and 3D. We present the thirty exponential integrators in Section 2 and the fourteen model problems in Section 3. The numerical results in Section 4 show that it is hard to do much better than one of the simplest of these formulas, the ETDRK4 scheme of Cox and Matthews [12].

2. Thirty exponential integrators.

2.1. Exponential general linear methods. We consider exponential integrators, based on the approximation of the Jacobian of (1.8), that belong to the large class of exponential general linear methods, first introduced by Minchev and Wright in 2005 [39]. This class contains, in particular, the ETD Runge-Kutta (one-step), ETD Adams-Bashforth (multistep), Lawson and exponential predictor-corrector methods. For given starting values $\hat{u}_0, \hat{u}_1, \dots, \hat{u}_{q-1}$ at times $t = 0, h, \dots, (q-1)h$, the numerical approximation \hat{u}_{n+1} at time $t_{n+1} = (n+1)h$, $n+1 \geq q$, is given by the formula

$$\hat{u}_{n+1} = e^{h\mathbf{L}}\hat{u}_n + h \sum_{i=1}^s B_i(h\mathbf{L})\mathbf{N}(\hat{v}_i) + h \sum_{i=1}^{q-1} V_i(h\mathbf{L})\mathbf{N}(\hat{u}_{n-i}), \quad (2.1)$$

C_2	$A_{2,1}$			$U_{2,1}$	\dots	$U_{2,q-1}$	
\vdots	\vdots	\ddots		\vdots		\vdots	
C_s	$A_{s,1}$	\dots	$A_{s,s-1}$	$U_{s,1}$	\dots	$U_{s,q-1}$	
	B_1	\dots	B_{s-1}	B_s	V_1	\dots	V_{q-1}

TABLE 2.1

Butcher tableau for the coefficients of an exponential integrator with q steps and s stages.

with q steps \hat{u}_{n-i} and s stages \hat{v}_i , with $\hat{v}_1 = \hat{u}_n$ and

$$\hat{v}_i = e^{C_i h \mathbf{L}} \hat{u}_n + h \sum_{j=1}^{i-1} A_{i,j}(h \mathbf{L}) \mathbf{N}(\hat{v}_j) + h \sum_{j=1}^{q-1} U_{i,j}(h \mathbf{L}) \mathbf{N}(\hat{u}_{n-j}), \quad 2 \leq i \leq s. \quad (2.2)$$

Note that, in practice, the nonlinear evaluations $\mathbf{N}(\hat{v}_i)$ and $\mathbf{N}(\hat{u}_{n-i})$ are carried out in value space, e.g., $\mathbf{N}(\hat{v}_i)$ means $\mathcal{F}(\mathbf{N}(\mathcal{F}^{-1} \hat{v}_i))$, with discrete Fourier transform \mathcal{F} . Methods of the form (2.1)–(2.2) not only include purely one-step methods ($q = 1$, $s \geq 1$) and purely multistep methods ($q \geq 1$, $s = 1$), but also combinations of both. Each scheme is characterised by its coefficients A , B , C , U , and V , which can be conveniently listed in a Butcher tableau, see Table 2.1. Note that these coefficients (except C) depend on \mathbf{L} —for instance, (1.5) uses one stage and one step, and its only non-zero coefficient is $B_1 = \varphi_1(h \mathbf{L})$.

The coefficients satisfy the following summation properties⁵,

$$\begin{aligned} B_1 &= \varphi_1(h \mathbf{L}) - \sum_{i=2}^s B_i(h \mathbf{L}) - \sum_{i=1}^{q-1} V_i(h \mathbf{L}), \\ A_{i,1} &= \psi_{1,i}(h \mathbf{L}) - \sum_{j=2}^{i-1} A_{i,j}(h \mathbf{L}) - \sum_{j=1}^{q-1} U_{i,j}(h \mathbf{L}), \quad 2 \leq i \leq s, \end{aligned} \quad (2.3)$$

where the φ - and ψ -functions are exponential and related functions that we shall define in the next subsection. As a consequence, it is notationally convenient to incorporate this condition by filling the corresponding entries of the Butcher tableau with a dot on the understanding that these method coefficients are given by (2.3). Note that the exponential integrators of the form (2.1)–(2.2) do not include the Exponential Propagation Iterative methods of Runge-Kutta type (EPIRK) [43, 44, 51, 52, 54] and the EMAM4 scheme of Calvo and Palencia [9]. The second author showed in [6] that the former—derived with the use of Krylov methods in mind where they perform well—are less competitive in this context, and that the latter often suffers from stability problems.

Let us finish this section with a few words about the computational cost per time-step. Since the matrices in (2.1)–(2.2) are diagonal, the matrix-vector products cost only $O(N)$ operations, where N is the number of grid points. The dominant cost per time-step is then the cost of an FFT [11], i.e., $O(N \log N)$ operations.

2.2. Evaluating the φ -functions. The coefficients A , B , C , U , and V involve the φ and ψ -functions applied to \mathbf{L} . Because \mathbf{L} is diagonal, $\varphi(\mathbf{L})$ and $\psi(\mathbf{L})$ reduce to φ and ψ applied to the diagonal elements of \mathbf{L} , so all we have to be able to is to compute $\varphi(\lambda)$ and $\psi(\lambda)$ for $\lambda \in \mathbb{C}$. The

⁵There are two exceptions: the coefficients of the Lawson4 and ABLawson4 schemes do not satisfy (2.3).

φ -functions are defined by the recurrence relation,

$$\varphi_{l+1}(z) = \frac{\varphi_l(z) - 1/l!}{z}, \quad l \geq 1, \quad (2.4)$$

with $\varphi_0(z) = e^z$. After φ_0 , the first few φ -functions are (1.6) and

$$\varphi_2(z) = \frac{e^z - z - 1}{z^2}, \quad \varphi_3(z) = \frac{e^z - \frac{z^2}{2} - z - 1}{z^3}, \quad (2.5)$$

while the ψ -functions are defined via the φ -functions and the coefficients C ,

$$\psi_{l,m}(z) = C_m^l \varphi_l(C_m z), \quad l \geq 0, \quad 1 \leq m \leq s. \quad (2.6)$$

Equations (2.4) and (2.6) can be implemented recursively, but the accurate evaluation of φ and ψ is not straightforward because it can suffer from cancellation error. Following the idea of Kassam and Trefethen in [29], to compute the functions at some $\lambda \in \mathbb{C}$, we use Cauchy's integral formula

$$\varphi(\lambda) = \frac{1}{2\pi i} \oint_{\Gamma} \frac{\varphi(z)}{z - \lambda} dz, \quad (2.7)$$

which can be approximated with exponential accuracy by the trapezoidal rule [58],

$$\varphi(\lambda) \approx \frac{1}{M} \sum_{k=1}^M \varphi(\lambda + e^{2\pi i(k-0.5)/M}), \quad (2.8)$$

taking Γ to be the circle of radius 1 centred at λ , oriented counter-clockwise, discretized with M equally spaced points. Note that the φ -functions satisfy $\varphi(\bar{z}) = \bar{\varphi}(z)$ for all $z \in \mathbb{C}$. As a consequence, when λ is on the real axis, we can take Γ to be the upper half of the circle of radius 1 centred at λ and take the real part of the result, i.e.,

$$\varphi(\lambda) = \frac{1}{\pi} \mathcal{R} \left(\int_0^\pi \varphi(\lambda + e^{i\theta}) d\theta \right), \quad (2.9)$$

which can be discretized by

$$\varphi(\lambda) \approx \frac{1}{M} \mathcal{R} \left(\sum_{k=1}^M \varphi(\lambda + e^{\pi i(k-0.5)/M}) \right). \quad (2.10)$$

If this symmetry is not explicitly used in the computation of the φ -functions when λ is real, rounding errors appear that lead to numerical instability.

Using contour integrals is not the only possible remedy for cancellation error. When Pope introduced (1.5), he suggested the use of Taylor series for small λ and the direct formula for large λ . The problem with this approach is that, for some intermediate values, neither method gives full precision, as noted by Cox and Matthews [12] and Kassam and Trefethen [29]. Another approach is to use Padé approximations, combined with a scaling and squaring technique [5]. This method is also effective, but the contour integral method is particularly appealing because of its greater generality for dealing with arbitrary functions.

Method	Type	Order	Stages s	Steps q	Ref.
ABNørsett4	ETD Adams-Bashforth	4	1	4	[40]*
ABNørsett5	ETD Adams-Bashforth	5	1	5	[40]*
ABNørsett6	ETD Adams-Bashforth	6	1	6	[40]*
ETDRK4	ETD Runge-Kutta	4	4	1	[12]
Friedli	ETD Runge-Kutta	4	4	1	[15]
Krogstad	ETD Runge-Kutta	4	4	1	[31]
Minchev	ETD Runge-Kutta	4	4	1	[38]
Strehmel-Weiner	ETD Runge-Kutta	4	4	1	[27]
Hochbruck-Ostermann	ETD Runge-Kutta	4	5	1	[23]
EXPRK5S8	ETD Runge-Kutta	5	8	1	[35]
ABLawson4	Lawson	4	1	4	[33]
Lawson4	Lawson	4	4	1	[33]
GenLawson41	Gen. Lawson	4	4	1	[31]
GenLawson42	Gen. Lawson	4	4	2	[31]
GenLawson43	Gen. Lawson	4	4	3	[31]
GenLawson44	Gen. Lawson	5	4	4	[31]
GenLawson45	Gen. Lawson	6	4	5	[31]
ModGenLawson41	Mod. Gen. Lawson	4	4	1	[41]*
ModGenLawson42	Mod. Gen. Lawson	4	4	2	[41]*
ModGenLawson43	Mod. Gen. Lawson	4	4	3	[41]*
ModGenLawson44	Mod. Gen. Lawson	5	4	4	[41]*
ModGenLawson45	Mod. Gen. Lawson	6	4	5	[41]*
PEC423	Exp. predictor-corrector	4	2	3	[41]*
PECEC433	Exp. predictor-corrector	4	3	3	[41]*
PEC524	Exp. predictor-corrector	5	2	4	[41]*
PECEC534	Exp. predictor-corrector	5	3	4	[41]*
PEC625	Exp. predictor-corrector	6	2	5	[41]*
PECEC635	Exp. predictor-corrector	6	3	5	[41]*
PEC726	Exp. predictor-corrector	7	2	6	[41]*
PECEC736	Exp. predictor-corrector	7	3	6	[41]*

TABLE 2.2

A reference table for the exponential integrators considered in this article. Note that some methods do not appear explicitly in the references listed but can be derived using order conditions or recurrence formulas found there; these cases are marked by asterisks. The Butcher tableaux for all of these formulas can be found in the supplementary material.

2.3. Introducing the thirty exponential integrators. Table 2.2 lists the exponential integrators considered in this paper. The Butcher tableaux can be found in in the supplementary material.

The first category of exponential integrators is the *ETD Adams-Bashforth* schemes of orders four to six. These are ETD (purely) multistep methods, which reduce to Adams-Bashforth schemes when $\mathbf{L} = 0$, and go back to Nørsett in 1969 [40]. Since $s = 1$, (2.1)–(2.2) reduces to

$$\hat{u}_{n+1} = e^{h\mathbf{L}}\hat{u}_n + hB_1(h\mathbf{L})\mathbf{N}(\hat{u}_n) + h \sum_{i=1}^{q-1} V_i(h\mathbf{L})\mathbf{N}(\hat{u}_{n-i}), \quad (2.11)$$

i.e., the only non-zero coefficients are B_1 and the V 's. Note that since \hat{u}_{n-i} and $\mathbf{N}(\hat{u}_{n-i})$ have been already computed, (2.11) only requires two FFT's per time-step since $\mathbf{N}(\hat{u}_n) = \mathcal{F}(\mathbf{N}(\mathcal{F}^{-1}\hat{u}_n))$.

$\frac{1}{2}$	·			
$\frac{1}{2}$	·	$\psi_{1,2}$		
1	·	0	$2\psi_{1,2}$	
	·	$2\varphi_2 - 4\varphi_3$	$2\varphi_2 - 4\varphi_3$	$-\varphi_2 + 4\varphi_3$

TABLE 2.3

Butcher tableau for *ETDRK4*. Note the dots in the first column, which indicate that these coefficients are computed using (2.3).

We label these methods as *ABNørsett q* , where $4 \leq q \leq 6$ is the order and also the number of steps. For more details on the derivation of *ABNørsett* methods see Minchev and Wright [39], who also show a connection between these schemes and the *IMEX* schemes of Ascher, Ruuth and Wetton [3]. One can also derive methods based on Adams-Moulton methods, known as *AMNørsett q* methods. These are implicit but can be used within predictor-corrector pairs, as we will see when introducing exponential predictor-corrector schemes (the last category in the table). A comprehensive look at both the Adams-Bashforth and Adams-Moulton exponential integrators can be found in the paper by Hochbruck and Ostermann [25].

The second category is the *ETD Runge-Kutta* schemes of order four to five. These are (purely) one-step methods and go back to Friedli in 1978 [15] and Strehmel-Weiner in 1982 [27]. More recently, inspired by Cox and Matthews' *ETDRK4* scheme [12], Minchev [38] in 2004 and Krogstad [31] and Hochbruck and Ostermann [23] in 2005 derived *ETD Runge-Kutta* schemes of order four. Luan and Ostermann proposed a scheme of order five (*EXPRK5S8*) in 2014 [35]. Overviews of *ETD Runge-Kutta* methods and some of their history can be found in the reviews of Hochbruck and Ostermann [24] and Minchev and Wright [39], where connections are described between *ETD Runge-Kutta*, generalised *Runge-Kutta* and semi-implicit methods. Since $q = 1$, (2.1)–(2.2) reduces to

$$\begin{aligned} \hat{u}_{n+1} &= e^{h\mathbf{L}}\hat{u}_n + h \sum_{i=1}^s B_i(h\mathbf{L})\mathbf{N}(\hat{v}_i), \\ \hat{v}_1 &= \hat{u}_n, \quad \hat{v}_i = e^{C_i h\mathbf{L}}\hat{u}_n + h \sum_{j=1}^{i-1} A_{i,j}(h\mathbf{L})\mathbf{N}(\hat{v}_j), \quad 2 \leq i \leq s. \end{aligned} \tag{2.12}$$

The only non-zero coefficients are the *A*'s, the *B*'s and the *C*'s. The coefficients for the *ETDRK4* scheme can be found in Table 2.3. Note that (2.12) requires $2s$ FFT's per time-step.

The third category is the *Lawson* methods. First developed by Lawson in 1967 [33], and often known as integrating factor (*IF*) methods, the motivation behind *Lawson* methods is to use a change of variable in (1.2) to get rid of the stiff linear part, and then apply a numerical solver to the transformed equation. The *Lawson* transformation consists of the change of variables $v(t) = e^{-\mathbf{L}t}u(t)$. If we differentiate this and substitute into (1.2), the transformed equation is

$$v' = e^{-\mathbf{L}t}\mathbf{N}(e^{\mathbf{L}t}v), \quad v(0) = u_0. \tag{2.13}$$

The linear term is gone, and the transformed equation (2.13), while no longer stiff, now has rapidly varying coefficients. Once we have decided on a scheme to solve (2.13), we can transform back to u . Lawson, in his 1967 paper, used the classical fourth order *Runge-Kutta* scheme on the transformed equation (2.13); we call this method *Lawson4*. Using the classical fourth order Adams-Bashforth

scheme gives the ABLawson4 method. Ehle and Lawson observed in [14] that Runge-Kutta based Lawson methods only work well when the problem is moderately stiff. Another problem with Lawson methods, as indicated by Krogstad [31], is that they do not preserve fixed points of the differential equation. Krogstad worked around these problems to derive generalised Lawson methods, also called generalised integrating factor (GIF) methods, the fourth category in the table.

Generalised Lawson methods are based on the transform

$$v(t) = e^{-\mathbf{L}t}u(t) - e^{-\mathbf{L}t} \sum_{l=1}^q t^l \varphi_l(t\mathbf{L})p_{l-1}, \quad (2.14)$$

where the p_l are the coefficients, in a (scaled) monomial basis, of the polynomial $P(t)$ of degree $q-1$ that interpolates the values $\{N(u_{n-l})\}_{l=1}^q$ at the points $\{t_{n-l}\}_{l=1}^q$; see [24, 39] for details. Differentiating this and substituting into (1.2) leads to the transformed equation

$$v' = e^{-\mathbf{L}t} \left(\mathbf{N} \left(e^{\mathbf{L}t}v + \sum_{l=1}^q t^l \varphi_l(t\mathbf{L})p_{l-1} \right) - P(t) \right), \quad v(0) = u_0. \quad (2.15)$$

Note that (2.13) is the special case of (2.15) with $P(t) = 0$. The idea of Krogstad is to apply, for various values of q , the classical fourth order Runge-Kutta scheme on (2.15), and then transform back to u . It leads to methods with four stages and q steps, called the GenLawson4 q methods.

As we increase q in the generalised Lawson methods we incorporate more of the nonlinearity and the methods have improved accuracy. However, this in part comes at the cost of stability, especially for dispersive problems, as was demonstrated by Krogstad [31]. A modification, based on satisfying order conditions, given by Ostermann, Thalhammer and Wright [41], significantly improves stability. The modification is given by the requirement that

$$\sum_{i=1}^4 B_i(h\mathbf{L}) \frac{c_i^j}{j!} + \sum_{i=1}^{q-1} V_i(h\mathbf{L}) \frac{(-1)^j}{j!} = \varphi_{j+1}(h\mathbf{L}), \quad 0 \leq j \leq q-1, \quad (2.16)$$

where, as before, $q-1$ is the degree of the polynomial approximation. These are the *modified generalised Lawson* methods, labelled as ModGenLawson4 q .

Just as with the standard Adams-Bashforth and Adams-Moulton multistep methods, the exponential versions can be used in predictor-corrector pairs. These are the *exponential predictor-corrector* methods, the last category in the table. For instance, using ABNørsett3 for a predictor step and AMNørsett4 for the corrector step yields the fourth order method called PEC423 in the MATLAB package EXPINT [4]. (PEC stands for predict-evaluate-correct, four is the order, two is the number of stages and three is the number of steps.) One can evaluate and correct again, that is, use the corrector twice. The name PECEC433 is given in EXPINT for the fourth order method that uses ABNørsett3 for a predictor step and AMNørsett4 for two corrector steps. We will also consider corrector steps applied three times.

3. Fourteen model problems. In this section we describe the PDEs (and their initial conditions) used in the numerical comparisons of Section 4. There are six PDEs in 1D and four PDEs considered in both 2D and 3D.

3.1. Model problems in 1D. The *Allen-Cahn equation*, derived by Allen and Cahn in the 1970s, is a reaction-diffusion equation which describes the process of phase separation in iron alloys

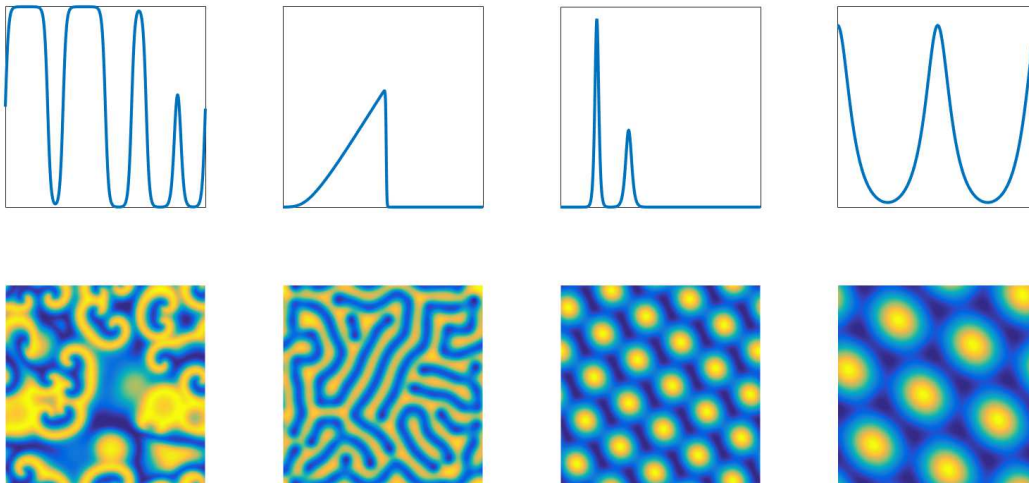


FIG. 3.1. First row, from left to right: a metastable solution of the Allen-Cahn equation (3.1), a smoothed shock of the viscous Burgers equation (3.4), a two-soliton solution of the KdV equation (3.10) and the absolute value of a breather solution of the nonlinear Schrödinger equation (3.19). Second row, from left to right: the real part of a spiral wave solution of the 2D Ginzburg-Landau equation (3.23), a fingerprint pattern solution of the 2D Gray-Scott equations (3.26) and two spot pattern solutions of the 2D Schnakenberg (3.29) and the 2D Swift-Hohenberg equations (3.32).

(see, e.g., [2]). It is given in one dimension as

$$u_t = \epsilon u_{xx} + u - u^3, \quad (3.1)$$

with linear diffusion ϵu_{xx} and a cubic reaction term $u - u^3$. The function u is the order parameter, a correlation function related to the positions of the different components of the alloy. The Allen-Cahn equation exhibits stable equilibria at $u = \pm 1$ while $u = 0$ is an unstable equilibrium. Solutions often display metastability where wells $u \approx -1$ compete with peaks $u \approx 1$, and structures remain almost unchanged for long periods of time before changing suddenly. This can be quantified: features with width L persist for time scales on the order of $e^{L/\epsilon}$. In Fourier space, (3.1) becomes

$$\hat{u}' = -\epsilon k^2 \hat{u} + \hat{u} - \mathcal{F}((\mathcal{F}^{-1} \hat{u})^3). \quad (3.2)$$

Note that $-k^2 \hat{u}$ is an abuse of notation and means $\mathbf{D}^{(2)} \hat{u}$. We take $\epsilon = 5 \times 10^{-2}$,

$$u(0, x) = \frac{1}{3} \tanh(2 \sin(x)) - e^{-23.5 \cdot (x - \pi/2)^2} + e^{-27(x - 4.2)^2} + e^{-38(x - 5.4)^2}, \quad x \in [0, 2\pi], \quad (3.3)$$

and solve up to $t = 40$. This initial condition quickly converges to a set of wells $u \approx -1$ and peaks $u \approx 1$ (at around $t = 4$) and eventually to a two-plateau solution (at around $t = 500$). Figure 3.1 shows the solution at time $t = 113$, when the peak on the far right is switching to $u \approx -1$.

Proposed by Burgers in 1948 to model turbulence in fluid dynamics [7], the *viscous Burgers equation*,

$$u_t = \epsilon u_{xx} - uu_x = \epsilon u_{xx} - \frac{1}{2}(u^2)_x, \quad (3.4)$$

ouples linear diffusion ϵu_{xx} with nonlinear convection $-uu_x$. It is the one-dimensional version of the momentum equation of the Navier-Stokes equations, with the pressure term dropped. The function u represents the velocity field. The limit $\epsilon \rightarrow 0$, the inviscid Burgers equation, admits solutions with discontinuities, which are termed *shocks*. When $\epsilon \neq 0$, diffusion competes with shock formation. In Fourier space, (3.4) becomes

$$\hat{u}' = -\epsilon k^2 \hat{u} - \frac{ik}{2} \mathcal{F}((\mathcal{F}^{-1} \hat{u})^2). \quad (3.5)$$

We take $\epsilon = 10^{-3}$,

$$u(0, x) = (1 - x^2)e^{-30(x+1/2)^2}, \quad x \in [-1, 1], \quad (3.6)$$

and solve up to $t = 1$. This initial condition steepens until $t \approx 0.5$ but eventually diffuses to its mean value at larger t . Figure 3.1 shows the solution at time $t = 1$.

The *Cahn-Hilliard equation*,

$$u_t = D(-u_{xx} - \gamma u_{xxxx} + (u^3)_{xx}), \quad (3.7)$$

is a fourth order reaction-diffusion problem which Cahn and Hilliard suggested in 1958 as a model for the process of phase separation in binary alloys [8]. It couples second-order destabilizing diffusion $-u_{xx}$ with fourth-order stabilizing diffusion $-u_{xxxx}$ and a differentiated cubic reaction term $(u^3)_{xx}$. The function u is defined as $u = 1 - 2c_A$ where $0 \leq c_A \leq 1$ and $c_B = 1 - c_A$ denote the concentrations of the two components A and B of the alloy, that is, $u = -1$ means pure A while $u = 1$ means pure B . The Cahn-Hilliard equation also exhibits metastable solutions. When quenched below a critical temperature, alloys described by (3.7) become unstable in the sense that small metastable pockets of relatively pure A and B may soon appear, corresponding to wells $u = -1$ and peaks $u = 1$. These pockets may coarsen into larger pockets at progressively larger times. In Fourier space, (3.7) becomes

$$\hat{u}' = D(k^2 - \gamma k^4) \hat{u} - Dk^2 \mathcal{F}((\mathcal{F}^{-1} \hat{u})^3). \quad (3.8)$$

We take $D = 10^{-2}$, $\gamma = 10^{-3}$,

$$u(0, x) = \frac{1}{5} \sin(4\pi x)^5 - \frac{4}{5} \sin(\pi x), \quad x \in [-1, 1], \quad (3.9)$$

and solve up to $t = 8$. This initial condition evolves to a four-plateau solution (two wells $u \approx -1$, two peaks $u \approx 1$) at around $t = 12$ before switching to a two-plateau solution (one well, one peak) at around $t = 70$.

The *Korteweg-de Vries (KdV) equation*,

$$u_t = -u_{xxx} - uu_x, \quad (3.10)$$

was derived by Korteweg and de Vries in 1895 to model the propagation of waves in shallow water [30]. It couples dispersion $-u_{xxx}$ with nonlinear convection $-uu_x$. Among the solutions of (3.10) are solitary waves or *solitons*. These are waves that maintain their shapes as they travel and are given by

$$u(t, x) = 3c \operatorname{sech}^2\left(\frac{\sqrt{c}}{2}(x - x_0 - ct)\right), \quad c > 0. \quad (3.11)$$

Waves of the form (3.11) have amplitude $3c$ and travel at constant speed c . This is contrast to solutions of linear wave equations $u_t = cu_x$, which all travel at velocity $-c$, regardless of their amplitudes. In Fourier space, (3.10) becomes

$$\hat{u}' = ik^3\hat{u} - \frac{ik}{2}\mathcal{F}((\mathcal{F}^{-1}\hat{u})^2). \quad (3.12)$$

We take

$$u(0, x) = 3A^2 \operatorname{sech}^2\left(\frac{A}{2}(x + 2)\right) + 3B^2 \operatorname{sech}^2\left(\frac{B}{2}(x + 1)\right), \quad x \in [-\pi, \pi], \quad (3.13)$$

with $A = 25$ and $B = 16$, and solve up to $t = 15 \times 10^{-3}$. This is a superposition of two solitons with speed A^2 and B^2 initially centred at $x = -2$ and $x = -1$, respectively. The stronger wave ($A = 25$) catches up with the weaker one ($B = 16$) at around $t = 10^{-3}$. Both waves remain unchanged after the interaction, the only nonlinear effect being a forward shift

$$\frac{1}{A^2} \log\left(\frac{A^2 + B^2}{A^2 - B^2}\right)^2 \quad (3.14)$$

for the stronger wave and a backward shift

$$-\frac{1}{B^2} \log\left(\frac{A^2 + B^2}{A^2 - B^2}\right)^2 \quad (3.15)$$

for the weaker one. The interaction ends at around $t = 3.5 \times 10^{-3}$. Figure 3.1 shows the initial condition.

The *Kuramoto-Sivashinsky equation*,

$$u_t = -u_{xx} - u_{xxxx} - uu_x, \quad (3.16)$$

dates to the mid-1970s with the work of Kuramoto [32] and Sivashinsky [47]. It couples destabilizing $-u_{xx}$ and stabilizing $-u_{xxxx}$ diffusions with nonlinear convection $-uu_x$. The nonlinear term shifts energy created at low wavenumbers by the second-order term to high wavenumbers where the fourth-order term stabilises. The Kuramoto-Sivashinsky equation models various physical phenomena, from unstable drift waves in plasmas to thermal instabilities in laminar flame fronts. In the latter, the function u represents the perturbation of the flame front surface. The solutions of (3.16) can demonstrate a wide range of spatio-temporal dynamics, including chaos. In Fourier space, (3.16) becomes

$$\hat{u}' = (k^2 - k^4)\hat{u} - \frac{ik}{2}\mathcal{F}((\mathcal{F}^{-1}\hat{u})^2). \quad (3.17)$$

We take

$$u(0, x) = \cos\left(\frac{x}{16}\right)\left(1 + \sin\left(\frac{x}{16}\right)\right), \quad x \in [0, 32\pi], \quad (3.18)$$

and solve up to $t = 30$. This simple initial data progressively evolves into a much more complicated superposition of wavenumbers and, even though the solution looks quite complicated, a characteristic pattern emerges from $t \approx 50$.

The (*focusing*) *nonlinear Schrödinger equation*,

$$u_t = iu_{xx} + i|u|^2u, \quad (3.19)$$

models several physical phenomena, including the nonlinear propagation of light in optical fibers. A nonlinear variant of the Schrödinger equation, it couples dispersion iu_{xx} with a nonlinear potential $i|u|^2u$. Note that the wave function u is complex-valued. Among the solutions of (3.19) are *breathers*, given by

$$u(t, x) = A \left(\frac{2B^2 \cosh(\theta) + 2iB\sqrt{2-B^2} \sinh(\theta)}{2 \cosh(\theta) - \sqrt{2}\sqrt{2-B^2} \cos(ABx)} - 1 \right) e^{iA^2t}, \quad \theta = A^2B\sqrt{2-B^2}t, \quad B \leq \sqrt{2}. \quad (3.20)$$

These are nonlinear waves in which energy concentrates in a localized and oscillatory fashion. In Fourier space, (3.19) becomes

$$\hat{u}' = -ik^2\hat{u} + i\mathcal{F}\left(|\mathcal{F}^{-1}\hat{u}|^2\mathcal{F}^{-1}\hat{u}\right). \quad (3.21)$$

We take

$$u(0, x) = \frac{2AB^2}{2 - \sqrt{2}\sqrt{2-B^2} \cos(ABx)} - A, \quad x \in [-\pi, \pi], \quad (3.22)$$

with $A = 2$ and $B = 1$, and solve up to $t = 1$. This is a breather whose amplitude oscillates in time around the value A . Figure 3.1 shows the initial condition.

3.2. Model problems in 2D and 3D. The (*complex*) *Ginzburg-Landau equation*,

$$u_t = (1 + iA)\Delta u + u - (1 + iB)u|u|^2, \quad (3.23)$$

was first derived in 2D by Stewartson and Stuart in 1971 to study non-linear instabilities in plane Poiseuille flow [48], using concepts from Ginzburg-Landau theory for superconductivity. The function u is the amplitude of a non-linear perturbation wave for values of the Reynolds number close to the critical value, above which perturbations may grow. Equation (3.23) admits solutions known as *frozen states* which correspond to quasi-frozen spiral defects surrounded by shock lines. In this regime, $|u|$ is stationary in time. We take $A = 0$ and $B = 1.5$, and if we take an initial condition of amplitude 0.1 involving random noise on the grid, it leads in both 2D and 3D to a frozen state solution at around $t = 10$. For the numerical comparisons of Section 4, we use

$$u(0, x, y) = e^{-0.1((x-50)^2+(y-50)^2)}, \quad (x, y) \in [0, 100]^2, \quad (3.24)$$

and

$$u(0, x, y, z) = e^{-0.1((x-50)^2+(y-50)^2+(z-50)^2)}, \quad (x, y, z) \in [0, 100]^3, \quad (3.25)$$

which also generate spiral waves, and solve up to $t = 10$ in both 2D and 3D. Figure 3.1 shows the 2D solution at $t = 30$ obtained with an initial condition of amplitude 0.1 involving random noise on the grid.

The *Gray-Scott equations*,

$$\begin{cases} u_t = \epsilon_u \Delta u + F(1 - u) - uv^2, \\ v_t = \epsilon_v \Delta v - (F + K)v + uv^2, \end{cases} \quad (3.26)$$

are reaction-diffusion equations derived by Gray and Scott in the early 1980s to study the properties of autocatalytic reactions [16, 17]. The system (3.26) models the chemical reaction $U + 2V \rightarrow 3V$; $V \rightarrow W$ with catalyst V ; u and v are the concentrations of U and V . Pure U is pumped into a stirred-tank reactor (at a constant flow rate F) inside which it reacts with V , and an exit pipe carries a mixture of U and V out (at the same rate F). The species U reacts with V ($-uv^2$ term), is pumped into the reactor (F) and carried out ($-Fu$). (Note that since the reaction uses U to generate V , the species U would eventually get exhausted if there were no replenishment.) The species V reacts with U (uv^2), generates W ($-Kv$) and is carried out ($-Fv$). These reactions are often complicated and can display various behaviours, such as *pattern formation*, including mitosis and fingerprint patterns. We take $\epsilon_u = 2 \times 10^{-5}$, $\epsilon_v = 10^{-5}$, $F = 3.5 \times 10^{-2}$ and $K = 6 \times 10^{-2}$. The initial conditions are

$$\begin{aligned} u(0, x, y) &= 1 - e^{-150((x-G/2.05)^2 + (y-G/2.05)^2)}, \\ v(0, x, y) &= e^{-150((x-G/2)^2 + 2(y-G/2)^2)}, \end{aligned} \quad (3.27)$$

with $(x, y) \in [0, G]^2$ and $G = 1.25$ in 2D, and

$$\begin{aligned} u(0, x, y, z) &= 1 - e^{-180((x-G/2.15)^2 + (y-G/2.15)^2 + (z-G/2.15)^2)}, \\ v(0, x, y, z) &= e^{-180((x-G/2)^2 + 2(y-G/2)^2 + 2(z-G/2)^2)}, \end{aligned} \quad (3.28)$$

with $(x, y, z) \in [0, G]^3$ and $G = 0.75$ in 3D. We solve up to $t = 60$ in 2D and $t = 50$ in 3D. These initial conditions, small perturbations from the constant solution $(u, v) = (1, 0)$, converge to a steady fingerprint pattern at around $t = 4500$ in 2D and $t = 2500$ in 3D. Figure 3.1 shows the 2D solution at $t = 4500$.

The *Schnakenberg equations*,

$$\begin{cases} u_t = \epsilon_u \Delta u + \gamma(a - u + u^2v), \\ v_t = \epsilon_v \Delta v + \gamma(b - u^2v), \end{cases} \quad (3.29)$$

are reaction-diffusion equations derived by Schnakenberg in 1979 to study limit cycle behaviours of two-component chemical reactions [46]. The system (3.29) models the chemical reaction $2U + V \rightarrow 3U$; $U \rightleftharpoons A$; $B \rightarrow V$; u and v are the concentrations of U and V , and A and B are another two chemical species, assumed to be maintained at constant concentrations a and b . We take $\epsilon_u = 1$, $\epsilon_v = 10$, $\gamma = 3$, $a = 0.1$ and $b = 0.9$. The initial conditions are

$$\begin{aligned} u(0, x, y) &= 1 - e^{-2((x-G/2.15)^2 + (y-G/2.15)^2)}, \\ v(0, x, y) &= .9/(.1^2 + .9^2) + e^{-2((x-G/2)^2 + 2(y-G/2)^2)}, \end{aligned} \quad (3.30)$$

with $(x, y) \in [0, G]^2$ and $G = 30$ in 2D, and

$$\begin{aligned} u(0, x, y, z) &= 1 - e^{-2((x-G/2.15)^2+(y-G/2.15)^2+(z-G/2.15)^2)}, \\ v(0, x, y, z) &= .9/(.1^2 + .9^2) + e^{-2((x-G/2)^2+2(y-G/2)^2+2(z-G/2)^2)}, \end{aligned} \quad (3.31)$$

with $(x, y, z) \in [0, G]^3$ and $G = 30$ in 3D. We solve up to $t = 20$ in both 2D and 3D. Note that these initial conditions are small perturbations from the constant solution $(u, v) = (a + b, b/(a^2 + b^2))$. They converge to a quasi-steady set of spots at around $t = 500$ in 2D and $t = 300$ in 3D. Figure 3.1 shows the 2D solution at $t = 500$.

The *Swift-Hohenberg equation*,

$$u_t = ru - (1 + \Delta)^2 u + \mathcal{N}(u), \quad (3.32)$$

with, e.g., $\mathcal{N}(u) = u^2 - u^3$, was first derived in 2D by Swift and Hohenberg in 1977 to study thermal fluctuations on a fluid near the Rayleigh-Bénard convective instability [50]. In 2D, the function u is the temperature field in a plane horizontal layer of fluid heated from below. Equation (3.32) is another example of a PDE that exhibits pattern formation, including stripes, spots and spirals. We take $r = 0.1$, and if we take an initial condition of amplitude 0.1 involving random noise on the grid, it leads in both 2D and 3D to a set of spots. For the numerical comparisons of Section 4, we use

$$u(0, x, y) = \frac{1}{4} \left(\sin(\pi x/10) + \sin(\pi y/10) + \sin(\pi x/2) \sin(\pi y/2) \right), \quad (x, y) \in [0, 20]^2, \quad (3.33)$$

and

$$\begin{aligned} u(0, x, y, z) &= \frac{1}{4} \left(\sin(\pi x/10) + \sin(\pi y/10) + \sin(\pi z/10) + \sin(\pi x/2) \sin(\pi y/2) \right. \\ &\quad \left. + \sin(\pi x/2) \sin(\pi z/2) + \sin(\pi y/2) \sin(\pi z/2) \right), \quad (x, y, z) \in [0, 20]^3, \end{aligned} \quad (3.34)$$

which also converge to a set of spots, and solve up to $t = 20$ in both 2D and 3D. Figure 3.1 shows the 2D solution at $t = 200$ obtained with an initial condition of amplitude 0.1 involving random noise on the grid.

4. Numerical comparisons. To compare exponential integrators, we follow the methodology of [29], though the experiments described here are far more extensive. We solve a given PDE up to $t = T$ for various time-steps h and a fixed number of grid points. We estimate the “exact” solution $u_{ex}(T, X)$ at $t = T$ by using a “very small” time-step (half the smallest time-step h) and the PECEC736 scheme (one of the two seventh-order accurate schemes in Table 2.2). The relative error between the computed solution $u_{comp}(T, X)$ and $u_{ex}(T, X)$ is then defined as

$$err = \frac{\|u_{comp}(T, X) - u_{ex}(T, X)\|_\infty}{\|u_{ex}(T, X)\|_\infty}. \quad (4.1)$$

For both u_{ex} and u_{comp} we use $N = 256$ grid points in 1D, $N_x N_y = 128^2$ grid points in 2D and $N_x N_y N_z = 32^3$ grid points in 3D. For the contours integrals, we use $M = 64$ points in 1D and $M = 32$ points in 2D and 3D. We plot (4.1) against relative time-steps h/T and computer times⁶

⁶Timings were done on a 2.7 GHz Intel i7 machine.

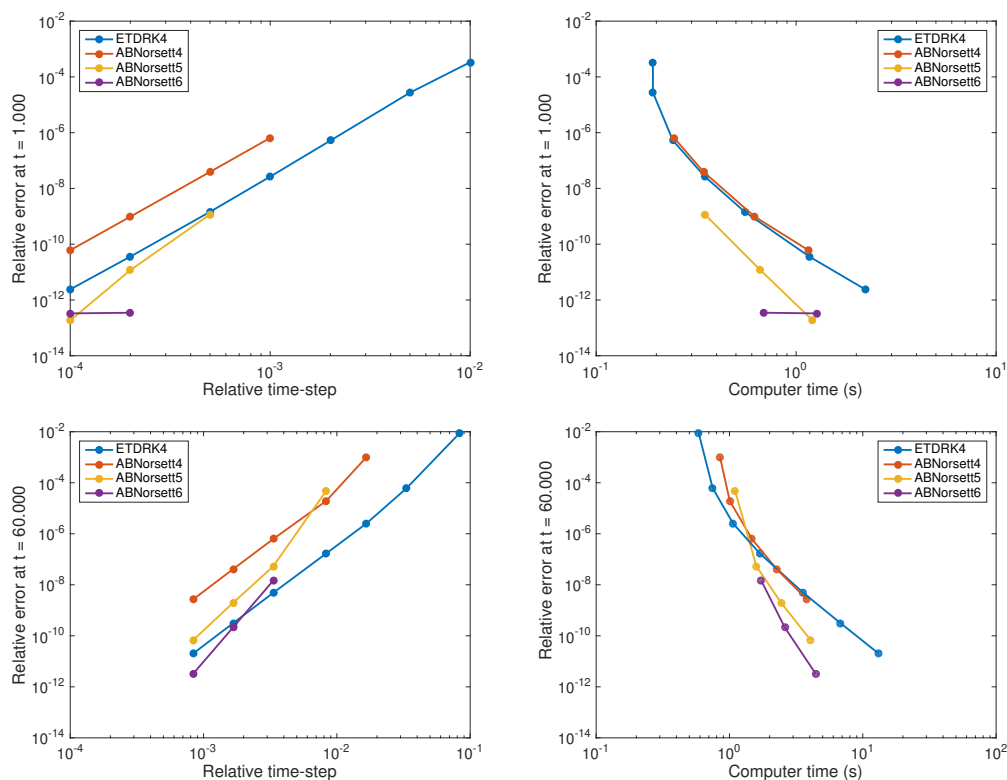


FIG. 4.1. Accuracy versus time-step and computer time for the ETD Adams-Bashforth methods for the 1D Burgers (top) and 2D Gray-Scott (bottom) equations. The order 5 and 6 methods are faster than ETDRK4 for high accuracies, but unstable at lower accuracies, as reflected in dots missing from the curves.

on a pair of graphs. The former gives a measure of the accuracy of the exponential integrator for various time-steps or, equivalently, for various number of integration steps. (If the relative time-step is 10^{-3} , it means that the integrator performed 10^3 steps to reach $t = T$.) However, it is possible that each step is more costly, so it is the latter which ultimately matters. We compare different families on different pairs of graphs with curves for ETDRK4 included on all plots as a baseline. Multistep methods with q steps are initialized with $q - 1$ iterations of the EXPRK5S8 scheme⁷ (the only fifth-order accurate one-step method in Table 2.2).

Figure 4.1 shows results for ETD Adams-Bashforth methods. These formulas are often unstable for large time-steps but can be competitive at high accuracies. The two graphs at the top correspond to the 1D Burgers equation (3.4). What we learn by looking at either of these graphs is that these integrators are highly unstable at large-time steps. (When dots are missing, it means the scheme was unstable.) We see that the fifth- and six-order methods (ABNørsett5 and ABNørsett6), when stable, are more accurate and faster than ETDRK4. Note that the ETDRK4 curve is almost

⁷This initialization step could, in theory, dominate the error. To be sure that is not the case in practice, we have initialized the multistep integrators with time-step h but also with time-steps $h/2$ and $h/4$, and have observed that it does not affect the error.

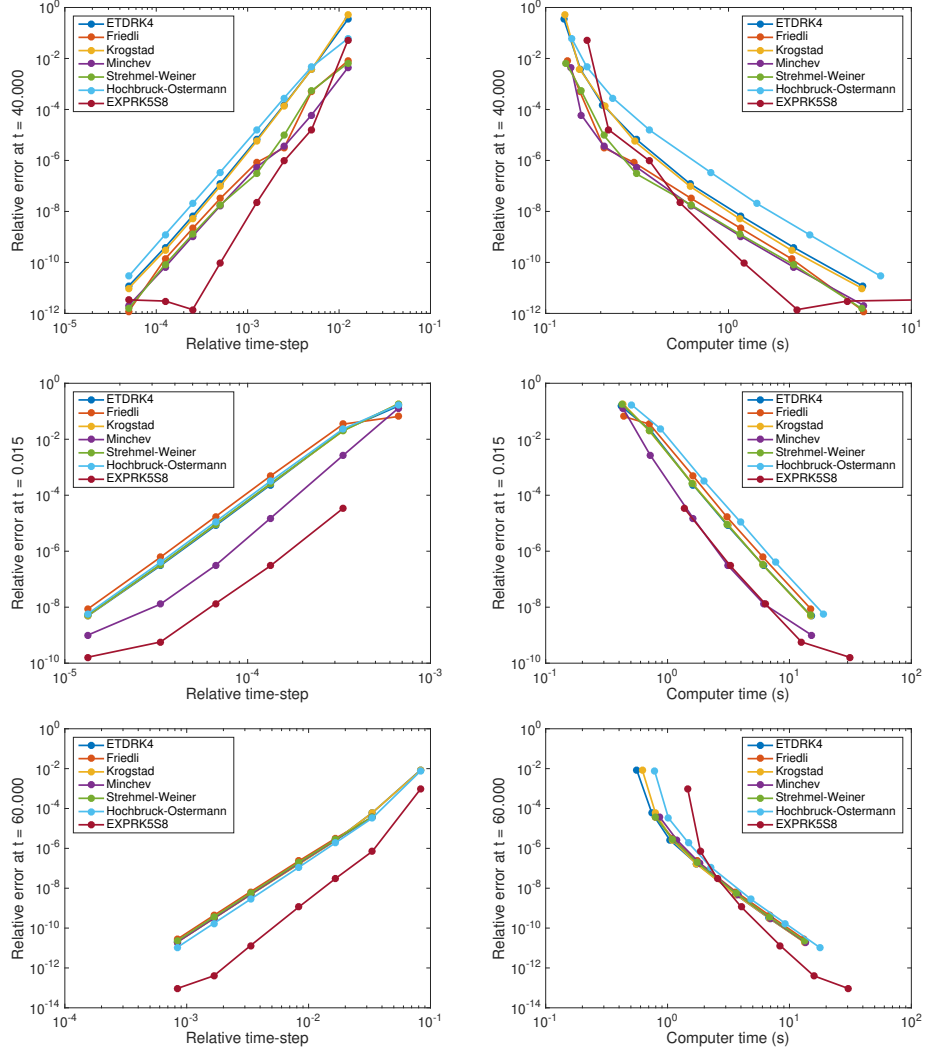


FIG. 4.2. Accuracy versus time-step and computer time for the ETD Runge-Kutta methods for the 1D Allen-Cahn (top), 1D KdV (center) and 2D Gray-Scott (bottom) equations. The EXPRK5S8 scheme is impressively fast, but unstable at low accuracies for the KdV equation and slow at low accuracies for the Gray-Scott equations.

vertical between the two first points. The reason is that for these two large time-steps, the dominant cost is the precomputation of the coefficients A and B . We reach similar conclusions looking at the two graphs at the bottom, which correspond to the 2D Gray-Scott equations (3.26): the ETD Adams-Bashforth methods are all unstable for large time-steps but the ABNørsett5 and ABNørsett6 methods are faster than ETD RK4 at high accuracies. This is not surprising since, as explained in Section 2, the cost per time-step of the ETD Adams-Bashforth methods is only two FFT's.

Figure 4.2 shows results for ETD Runge-Kutta methods. These formulas have good stability properties, and the fifth-order EXPRK5S8 integrator beats the fourth-order schemes at high ac-

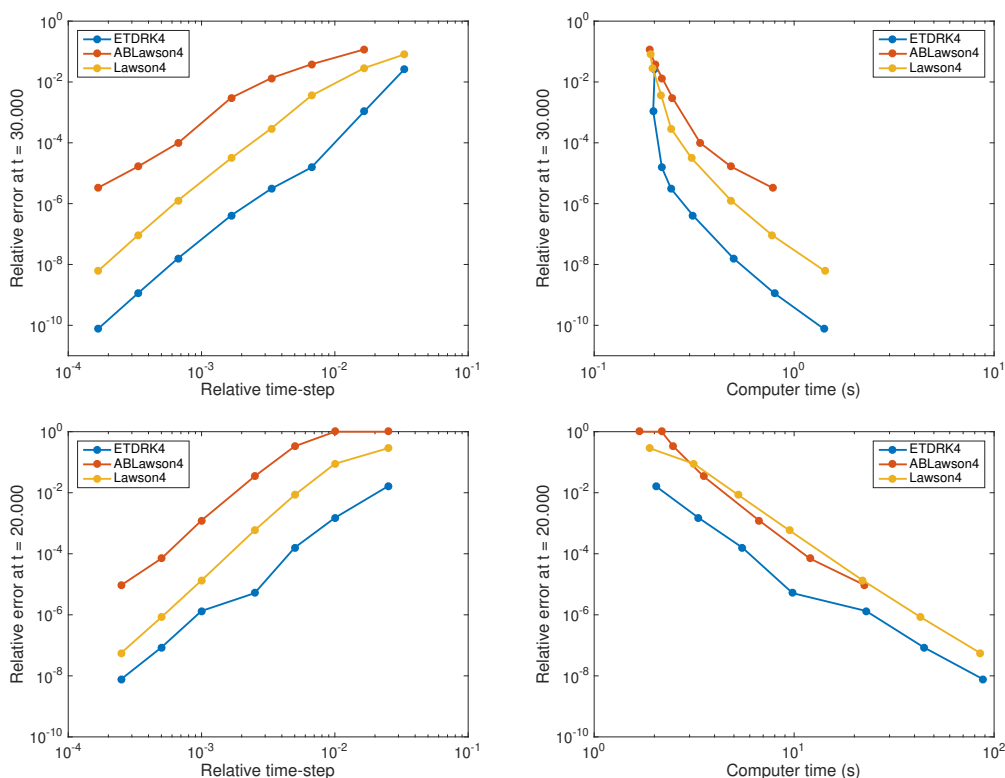


FIG. 4.3. Accuracy versus time-step and computer time for the Lawson methods for the 1D Kuramoto-Sivashinsky (top) and 3D Schnakenberg (bottom) equations. These formulas are too inaccurate to be competitive. The constants involved in the convergence bounds are too great.

curacies, but it exhibits instability for the KdV equation. The two graphs at the top correspond to the 1D Allen-Cahn equation (3.1). The integrators are stable and EXPRK5S8 beats ETDRK4 and the other fourth-order methods at high accuracies. If we look at the two graphs in the middle, which correspond to the 1D KdV equation (3.10), we observe that EXPRK5S8 is unstable for the largest time-step but is the fastest (with Minchev) when it is stable. For the 2D Gray-Scott equations (3.26) (bottom), the fifth-order EXPRK5S8 scheme is again the fastest at high accuracies, but is the slowest at lower accuracies. Note that the EXPRK5S8 integrator has eight stages, so it has a high cost per time-step, but it is so accurate that it is nonetheless competitive. On the other hand, the Hochbruck-Ostermann formula has five stages but is not more accurate than the other fourth-order schemes and hence is slower.

Figure 4.3 shows results for Lawson methods for the 1D Kuramoto-Sivashinsky and 3D Schnakenberg equations. These formulas are not accurate enough to be competitive. For the ABLawson4 formula, this lack of accuracy is slightly compensated by its speed (purely multistep hence faster per time-step), especially for the Schnakenberg equations.

Figure 4.4 shows results for generalised Lawson methods. These formulas suffer from instability but beat ETDRK4 at high accuracies when they are stable. For the Cahn-Hilliard equation (3.7),

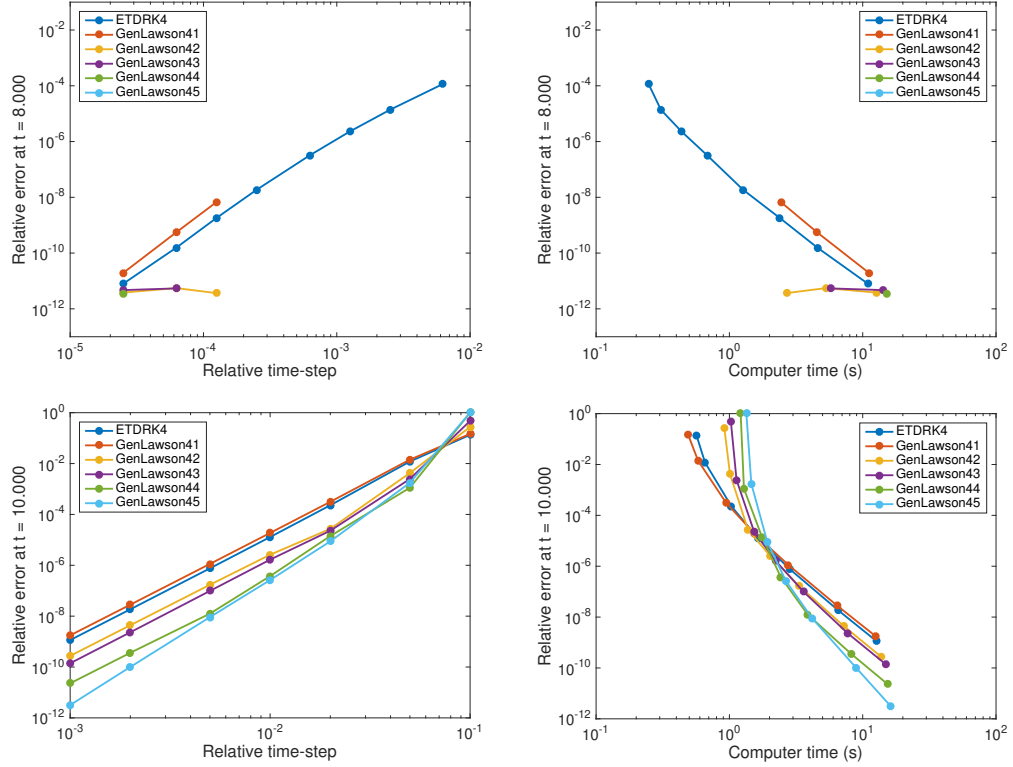


FIG. 4.4. Accuracy versus time-step and computer time for the generalised Lawson methods for the 1D Cahn-Hilliard (top) and 3D Ginzburg-Landau (bottom) equations. These methods perform well for some problems but are unstable for others at low accuracies.

the generalised Lawson methods are highly unstable but beat ETDRK4 for the smallest time-steps. For the 3D Ginzburg-Landau equation (3.23), they are stable and beat ETDRK4 at high accuracies. These methods have four stages and one to five steps, so their cost per time-step is relatively high, but their accuracy makes them competitive.

Figure 4.5 shows results for *modified generalised Lawson* methods. These formulas are much more stable than the generalized Lawson schemes and beat ETDRK4 at high accuracies. For the 1D nonlinear Schrödinger equation (3.19), they are slower at low accuracies but are faster at higher accuracies (expect ModGenLawson41). Same observations for the 2D Ginzburg-Landau equation (3.23): it is advantageous to use the modified generalised Lawson methods (especially ModGenLawson44 and ModGenLawson45) at high accuracies. Note that, like the generalised Lawson integrators, the modified generalised Lawson schemes have four stages and one to five steps, so it is their accuracy that makes them competitive.

Figure 4.6 shows results for *exponential predictor-corrector* methods. These formulas can be unstable for large time-steps but, when stable, are faster than ETDRK4. For the 1D Burgers equation (3.4), the exponential predictor-corrector methods are unstable for the largest (or two largest) time-steps (expect PEC433, stable for every time-steps). These integrators are however more accu-

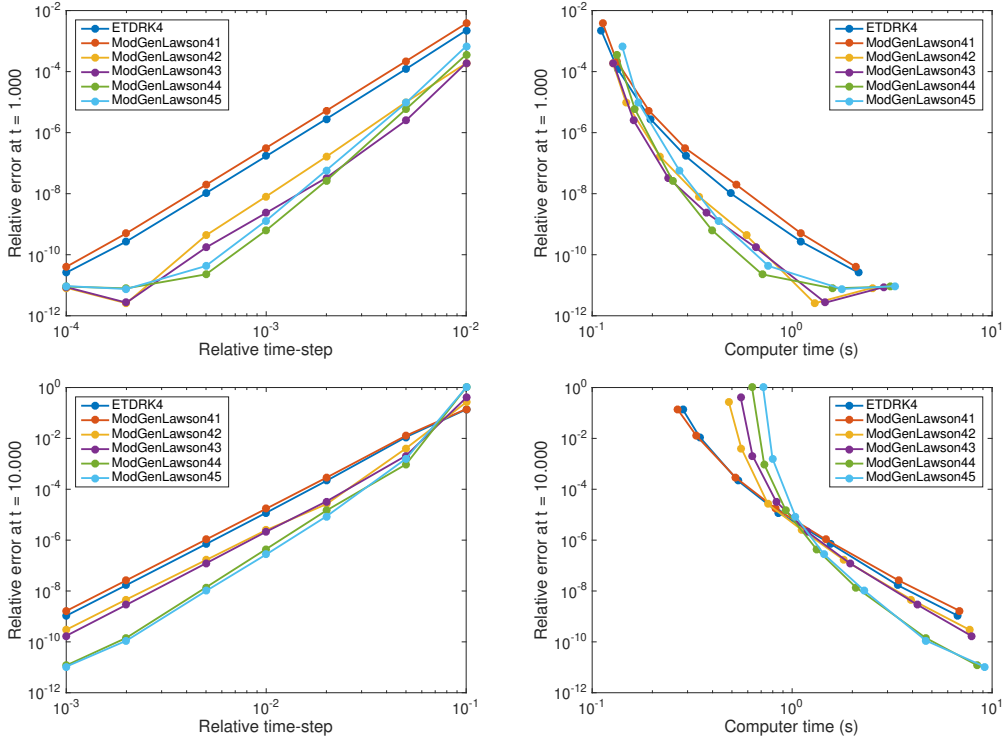


FIG. 4.5. Accuracy versus time-step and computer time for the modified generalised Lawson methods for the 1D nonlinear Schrödinger (top) and 2D Ginzburg-Landau (bottom) equations. The ModGenLawson41 formula has virtually identical performance to ETDRK4. The other variants are excellent at high accuracies but can be quite slow at low accuracies.

rate and faster. For the 3D Swift-Hohenberg equation (3.32), several exponential predictor-corrector schemes are also unstable for the largest time-step. In terms of accuracy, there is not much difference between these schemes and ETDRK4. In particular, the PEC726 and PECEC736 curves superimpose on the ETDRK4 curve. However, since PEC726 only uses two stages, it is faster than ETDRK4 per time-step and, having similar accuracy, is faster than ETDRK4 at high accuracies.

5. Discussion. The solution of PDEs by means of numerical methods is a wide and varied field. There are many types of methods just as there are many types of PDEs. For stiff time-dependent PDEs in 1D/2D/3D periodic domains, Fourier spectral methods with exponential integrators are the state-of-the-art algorithm. With the advent of software package such as Chebfun [13], we asked which integrator such packages should use for solving this class of problems. We have compared thirty exponential integrators on fourteen PDEs. The ideal solver should be accurate, fast and stable.

Our experiments show that the ETD Adams-Bashforth and the generalised Lawson methods are too unstable, while the Lawson methods are not accurate enough. Within the ETD Runge-Kutta methods, it is hard to do much better than ETDRK4. The fourth-order schemes are quite similar in terms of accuracy, speed and stability. The fifth-order EXPRK5S8 integrator is faster

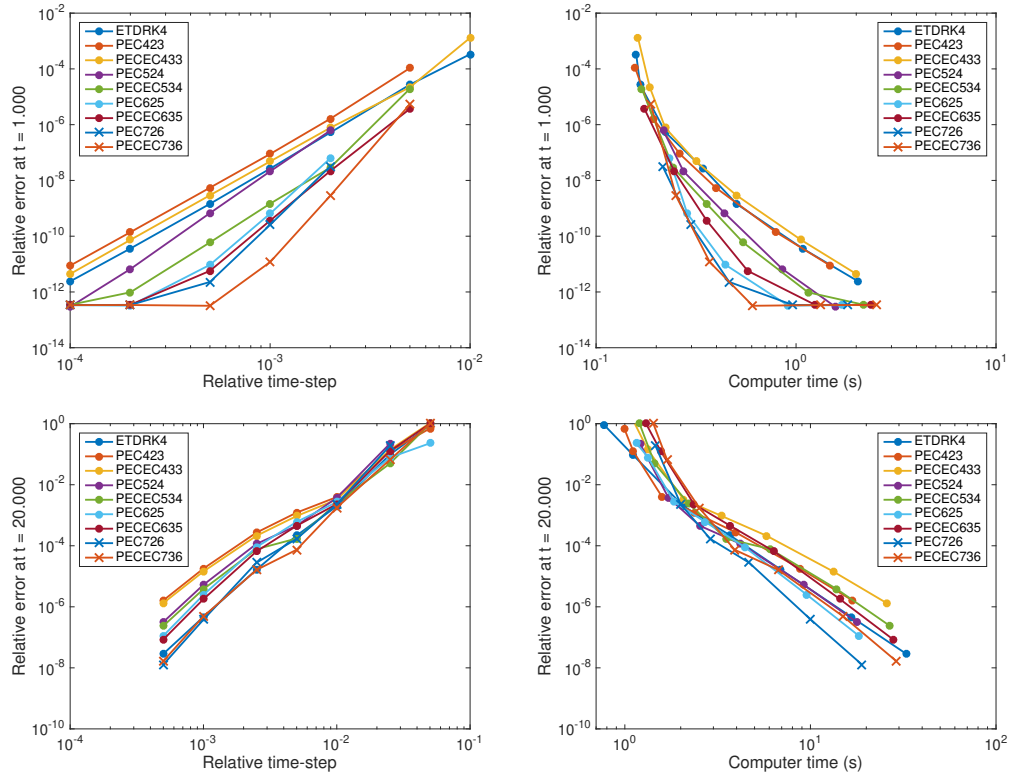


FIG. 4.6. Accuracy versus time-step and computer time for the exponential predictor-corrector methods for the 1D Burgers (top) and 3D Swift-Hohenberg (bottom) equations. These methods perform well in 1D, though slightly unstable at low accuracies. In 3D, they have virtually identical performance to ETDRK4 or are slower, except PEC726, faster at high accuracies.

at high accuracies. However, while looking for eight digits of accuracy in 1D is reasonable, it is probably less reasonable in 2D and 3D. It is unstable for the KdV equation and requires the precomputation of more than twice as many coefficients as ETDRK4, which makes it much more complicated to implement and probably less appealing to general users. The high-order modified generalised Lawson and exponential predictor-corrector methods are competitive stiff solvers at high accuracies, but the latter often suffers from instability for large time-steps. Note that these schemes are multistep formulas so they have to be initialised with one-step methods.

Our numerical experiments were done in Chebfun, a MATLAB-based package for computing with functions to about 15 digits of accuracy. Its extensions to periodic problems [61], 2D [55] and 3D [20] provide a very convenient framework for solving stiff PDEs in 1D/2D/3D periodic domains. More specifically, the `spin`, `spin2` and `spin3` codes implement a Fourier spectral method in space with an exponential integrator in time. The simplest way to see `spin` in action is to type simply `spin('ks')` (for the Kuramoto-Sivashinsky equation) or `spin2('gl2')` (for the 2D Ginzburg-Landau equation) or another similar string to invoke an example computation involving a preloaded initial condition and time interval. It is also possible to define a new PDE using the `spinop` class. To produce the graphs of Section 4, we have used the `spincomp` code—checkout

www.chebfun.org to learn more about `spin`, `spinop` and `spincomp`.

A potentially exciting application we have not considered here is the investigation of formation and stability of 3D quasicrystalline structures [49]. The formation of quasicrystals can be modelled by reaction-diffusion equations of the form (1.1), where the linear part \mathcal{L} is typically of order eight or ten.

Acknowledgements. This paper is dedicated to the celebration of Nick Trefethen on his 60th birthday and his inspirational contributions to the field of numerical analysis.

Appendix A: Trigonometric interpolation and Fourier spectral methods in 1D. Let $u(x)$ be a periodic function on $[0, 2\pi]$, possibly complex-valued. Let $\{x_j = 2\pi j/N\}$, $0 \leq j \leq N-1$, denote N equispaced points in $[0, 2\pi)$ and $\{u_j = u(x_j)\}$, $0 \leq j \leq N-1$, the values of u at the x_j 's. For an even number N , the trigonometric interpolant $p_N(x)$ of $u(x)$ at these points is defined by

$$p_N(x) = \sum'_{k=-N/2}^{N/2} \hat{u}_k e^{ikx}, \quad \hat{u}_k = \frac{1}{N} \sum_{j=0}^{N-1} u(x_j) e^{-ikx_j}, \quad -\frac{N}{2} \leq k \leq \frac{N}{2} - 1, \quad \hat{u}_{N/2} = \hat{u}_{-N/2}, \quad (5.1)$$

while, for an odd number N , it is defined by

$$p_N(x) = \sum_{k=-\frac{N-1}{2}}^{\frac{N-1}{2}} \hat{u}_k e^{ikx}, \quad \hat{u}_k = \frac{1}{N} \sum_{j=0}^{N-1} u(x_j) e^{-ikx_j}, \quad -\frac{N-1}{2} \leq k \leq \frac{N-1}{2}. \quad (5.2)$$

The prime on the summation sign in (5.1) signifies that the terms $k = \pm N/2$ are halved.

The philosophy of Fourier spectral methods (in coefficient space)⁸ is the following: interpolate $u(x)$ by $p_N(x)$ with Fourier coefficients \hat{u}_k , and to compute derivatives, multiply the \hat{u}_k 's by the appropriate power of ik . Since differentiation is a linear operation, it can be represented by matrices. The (diagonal) *first-order Fourier differentiation matrix* is the matrix which maps the Fourier coefficients of $p_N(x)$ to the Fourier coefficients of $p_N'(x)$, and has entries $[0, ik]$ with $|k| \leq N/2 - 1$ for N even and ik with $|k| \leq (N-1)/2$ for N odd. (Note that for N even, the first entry is 0, as opposed to $-iN/2$ ⁹.) More generally, for N odd and any $m \geq 1$, the m^{th} -order *Fourier differentiation matrix* has entries $(ik)^m$ with $|k| \leq (N-1)/2$. For N even and m odd, it has entries $[0, (ik)^m]$ with $|k| \leq N/2 - 1$, while for m even it has entries $(ik)^m$ with $-N/2 \leq k \leq N/2 - 1$.

At every time-step, we look for a solution of the form (5.1)–(5.2), so that the Fourier coefficients become functions of time t , as in (1.3)–(1.4).

Appendix B: Trigonometric interpolation and Fourier spectral methods in 2D and 3D. In 2D, we look for solutions of the form

$$u(t, x, y) \approx \sum'_{k=-\frac{N_x}{2}}^{\frac{N_x}{2}} \sum'_{l=-\frac{N_y}{2}}^{\frac{N_y}{2}} \hat{u}_{k,l}(t) e^{ikx} e^{ily}, \quad (x, y) \in [0, 2\pi]^2, \quad (5.3)$$

with N_x points $\{x_j = 2\pi j/N_x\}_{j=0}^{N_x-1}$ in the x -direction and N_y points $\{y_j = 2\pi j/N_y\}_{j=0}^{N_y-1}$ in the y -direction, and appropriate rescaling for different domains. The unknowns, at each time t , are the

⁸We describe in this section Fourier spectral methods in coefficient space. See [57] for details about Fourier spectral methods in value space.

⁹It is related to the derivative of the sawtooth wave on the grid being zero and not a complex exponential [57, Chapter 3].

$N_x N_y$ Fourier coefficients $\hat{u}_{k,l}(t)$, stored as a $N_x N_y \times 1$ vector. In 3D, we look for solutions of the form

$$u(t, x, y, z) \approx \sum'_{k=-\frac{N_x}{2}}^{\frac{N_x}{2}} \sum'_{l=-\frac{N_y}{2}}^{\frac{N_y}{2}} \sum'_{m=-\frac{N_z}{2}}^{\frac{N_z}{2}} \hat{u}_{k,l,m}(t) e^{ikx} e^{ily} e^{imz}, \quad (x, y, z) \in [0, 2\pi]^3, \quad (5.4)$$

with the same N_x and N_y points in the x and y directions, N_z points $\{z_j = 2\pi j/N_z\}_{j=0}^{N_z-1}$ in the z -direction, and appropriate rescaling for different domains. The unknowns, at each time t , are the $N_x N_y N_z$ Fourier coefficients $\hat{u}_{k,l,m}(t)$, stored as a $N_x N_y N_z \times 1$ vector. Again, the primes on the summation signs in (5.3)–(5.4) signify that the extreme terms are halved.

To construct the matrices \mathbf{L} , we use Kronecker products and the Fourier differentiation matrices of Appendix A. For example, in 2D, the Laplacian operator,

$$\mathcal{L}u = \Delta u = u_{xx} + u_{yy}, \quad (5.5)$$

is discretized by the $N_x N_y \times N_x N_y$ matrix

$$\mathbf{L} = \mathbf{I} \otimes \mathbf{D}^{(2)} + \mathbf{D}^{(2)} \otimes \mathbf{I}, \quad (5.6)$$

where \mathbf{I} is the identity matrix and $\mathbf{D}^{(2)}$ is the second-order Fourier differentiation matrix. Note that the first \mathbf{I} and the second $\mathbf{D}^{(2)}$ are $N_y \times N_y$ while the first $\mathbf{D}^{(2)}$ and the second \mathbf{I} are $N_x \times N_x$. Similarly, the two-dimensional biharmonic operator,

$$\mathcal{L}u = \Delta^2 u = u_{xxxx} + u_{yyyy} + 2u_{xxyy}, \quad (5.7)$$

is discretized by the $N_x N_y \times N_x N_y$ matrix

$$\mathbf{L} = \mathbf{I} \otimes \mathbf{D}^{(4)} + \mathbf{D}^{(4)} \otimes \mathbf{I} + 2(\mathbf{D}^{(2)} \otimes \mathbf{I})(\mathbf{I} \otimes \mathbf{D}^{(2)}), \quad (5.8)$$

where $\mathbf{D}^{(4)}$ is the fourth-order Fourier differentiation matrix, i.e., the matrix with entries k^4 . Again, one has to be careful with the dimensions of the matrices. In 3D, the Laplacian operator,

$$\mathcal{L}u = \Delta u = u_{xx} + u_{yy} + u_{zz}, \quad (5.9)$$

is discretized by the $N_x N_y N_z \times N_x N_y N_z$ matrix

$$\mathbf{L} = \mathbf{I} \otimes \mathbf{I} \otimes \mathbf{D}^{(2)} + \mathbf{I} \otimes \mathbf{D}^{(2)} \otimes \mathbf{I} + \mathbf{D}^{(2)} \otimes \mathbf{I} \otimes \mathbf{I}, \quad (5.10)$$

while the three-dimensional biharmonic operator,

$$\mathcal{L}u = \Delta^2 u = u_{xxxx} + u_{yyyy} + u_{zzzz} + 2u_{xxyy} + 2u_{xxzz} + 2u_{yyzz}, \quad (5.11)$$

is discretized by the $N_x N_y N_z \times N_x N_y N_z$ matrix

$$\begin{aligned} \mathbf{L} = & \mathbf{I} \otimes \mathbf{I} \otimes \mathbf{D}^{(4)} + \mathbf{I} \otimes \mathbf{D}^{(4)} \otimes \mathbf{I} + \mathbf{D}^{(4)} \otimes \mathbf{I} \otimes \mathbf{I} + 2(\mathbf{I} \otimes \mathbf{D}^{(2)} \otimes \mathbf{I})(\mathbf{I} \otimes \mathbf{I} \otimes \mathbf{D}^{(2)}) \\ & + 2(\mathbf{D}^{(2)} \otimes \mathbf{I} \otimes \mathbf{I})(\mathbf{I} \otimes \mathbf{I} \otimes \mathbf{D}^{(2)}) + 2(\mathbf{D}^{(2)} \otimes \mathbf{I} \otimes \mathbf{I})(\mathbf{I} \otimes \mathbf{D}^{(2)} \otimes \mathbf{I}), \end{aligned} \quad (5.12)$$

with matrices of appropriate dimensions. Note that Kronecker products can be computed in MATLAB with the `kron` command, and that the matrices (5.6)–(5.8)–(5.10)–(5.12) are diagonal.

REFERENCES

- [1] A. H. AL-MOHY AND N. J. HIGHAM, *Computing the action of the matrix exponential, with an application to exponential integrators*, SIAM J. Sci. Comput., 33 (2011), pp. 488–511.
- [2] S. M. ALLEN AND J. W. CAHN, *A microscopic theory for antiphase boundary motion and its application to antiphase domain coarsening*, Acta Metall., 27 (1979), pp. 1085–1095.
- [3] U. M. ASCHER, S. J. RUUTH, AND B. T. R. WETTON, *Implicit-explicit methods for time-dependent partial differential equations*, SIAM J. Numer. Anal., 32 (1995), pp. 797–823.
- [4] H. BERLAND, B. SKAFLESTAD, AND W. M. WRIGHT, *EXPINT—A MATLAB package for exponential integrators*, ACM Trans. Math. Softw. (TOMS), 33 (2007), pp. 4:1–4:17.
- [5] G. BEYKLIN, J. M. KEISER, AND L. VOZOVoi, *A new class of time discretization schemes for the solution of nonlinear PDEs*, J. Comput. Phys., 147 (1998), pp. 362–387.
- [6] N. J. BOOTLAND, *Exponential integrators for stiff PDEs*, Master’s thesis, University of Oxford, 2014.
- [7] J. M. BURGERS, *A mathematical model illustrating the theory of turbulence*, Advances in Applied Mechanics, 1 (1948), pp. 171–199.
- [8] J. W. CAHN AND J. E. HILLIARD, *Free energy of a nonuniform system. i. Interfacial free energy*, The Journal of Chemical Physics, 28 (1958), pp. 258–267.
- [9] M. P. CALVO AND C. PALENCIA, *A class of multistep exponential integrators for semilinear problems*, Numer. Math., 102 (2006), pp. 367–381.
- [10] J. CERTAINE, *The solution of ordinary differential equations with large time constants*, in Mathematical methods for digital computers, A. Ralston and H. S. Wilf, eds., Wiley, New York, 1960, pp. 128–132.
- [11] J. W. COOLEY AND J. W. TUKEY, *An algorithm for the machine calculation of complex Fourier series*, Math. Comp., 19 (1965), pp. 297–301.
- [12] S. M. COX AND P. C. MATTHEWS, *Exponential time differencing for stiff systems*, J. Comput. Phys., 176 (2002), pp. 430–455.
- [13] T. A. DRISCOLL, N. HALE, AND L. N. TREFETHEN, eds., *Chebfun Guide*, Pafnuty Publications, Oxford, 2014; see also www.chebfun.org.
- [14] B. L. EHLE AND J. D. LAWSON, *Generalized Runge-Kutta processes for stiff initial-value problems*, J. Inst. Maths. Appl., 16 (1975), pp. 11–21.
- [15] A. FRIEDLI, *Verallgemeinerte Runge-Kutta Verfahren zur Lösung steifer Differentialgleichungssysteme*, in Numerical Treatment of Differential Equations, R. Burlirsch, R. Grigorieff, and J. Schröder, eds., Springer, Berlin, 1978, pp. 35–50.
- [16] P. GRAY AND S. K. SCOTT, *Autocatalytic reactions in the isothermal, continuous stirred tank reactor: isolas and other forms of multistability*, Chem. Eng. Sci., 38 (1983), pp. 29–43.
- [17] ———, *Autocatalytic reactions in the isothermal, continuous stirred tank reactor: oscillations and instabilities in the system $A + 2B \rightarrow 3B; B \rightarrow C$* , Chem. Eng. Sci., 39 (1984), pp. 1087–1097.
- [18] E. HAIRER, G. BADER, AND C. LUBICH, *On the stability of semi-implicit methods for ordinary differential equations*, BIT, 22 (1982), pp. 211–232.
- [19] E. HAIRER AND G. WANNER, *Solving ordinary differential equations II*, Springer, Berlin, second ed., 1996.
- [20] B. HASHEMI AND L. N. TREFETHEN, *Chebfun in three dimensions*, manuscript in preparation.
- [21] J. HERSCH, *Contribution à la méthode des équations aux différences*, Z. Angew. Math. und Phys., 9 (1958), pp. 129–180.
- [22] M. HOCHBRUCK, C. LUBICH, AND H. SELHOFER, *Exponential integrators for large systems of differential equations*, SIAM J. Sci. Comput., 19 (1998), pp. 1552–1574.
- [23] M. HOCHBRUCK AND A. OSTERMANN, *Explicit exponential Runge-Kutta methods for semilinear parabolic problems*, SIAM J. Numer. Anal., 43 (2005), pp. 1069–1090.
- [24] ———, *Exponential integrators*, Acta Numer., 19 (2010), pp. 209–286.
- [25] ———, *Exponential multistep methods of Adams-type*, BIT, 51 (2011), pp. 889–908.
- [26] M. HOCHBRUCK, A. OSTERMANN, AND J. SCHWEITZER, *Exponential Rosenbrock-type methods*, SIAM J. Numer. Anal., 47 (2009), pp. 786–803.
- [27] S. K. AND R. WEINER, *Behandlung steifer Anfangswertprobleme gewöhnlicher Differentialgleichungen mit adaptiven Runge-Kutta-Methoden*, Computing, 29 (1982), pp. 153–165.
- [28] A.-K. KASSAM, *Solving reaction-diffusion equations 10 times faster*, Tech. Rep. 1192, Numerical Analysis Group, University of Oxford, 2003.
- [29] A.-K. KASSAM AND L. N. TREFETHEN, *Fourth-order time-stepping for stiff PDEs*, SIAM J. Sci. Comput., 26 (2005), pp. 1214–1233.
- [30] D. KORTEWEG AND G. D. VRIES, *On the change of form of long waves advancing in a rectangular canal, and on a new type of long stationary waves*, Philos. Mag. (Ser. 5), 39 (1895), pp. 422–443.

- [31] S. KROGSTAD, *Generalized integrating factor methods for stiff PDEs*, J. Comput. Phys., 203 (2005), pp. 72–88.
- [32] Y. KURAMOTO AND T. TSUZUKI, *Persistent propagation of concentration waves in dissipative media far from thermal equilibrium*, Progress of Theoretical Physics, 55 (1976), pp. 356–369.
- [33] J. LAWSON, *Generalized Runge-Kutta processes for stable systems with large Lipschitz constants*, SIAM J. Numer. Anal., 4 (1967), pp. 372–380.
- [34] J. LOFFELD AND M. TOKMAN, *Comparative performance of exponential, implicit, and explicit integrators for stiff systems of ODEs*, J. Comput. Appl. Math., 241 (2013), pp. 45–67.
- [35] V. T. LUAN AND A. OSTERMANN, *Explicit exponential Runge-Kutta methods of high order for parabolic problems*, J. Comput. Appl. Math., 256 (2014), pp. 168–179.
- [36] ———, *Exponential Rosenbrock methods of order five—construction, analysis and numerical comparisons*, J. Comput. Appl. Math., 255 (2014), pp. 417–431.
- [37] P. C. MATTHEWS, *Pattern formation on a sphere*, Phys. Rev. E, 67 (2003), p. 036206.
- [38] B. V. MINCHEV, *Exponential integrators for semilinear problems*, PhD thesis, University of Bergen, 2004.
- [39] B. V. MINCHEV AND W. M. WRIGHT, *A review of exponential integrators for first order semi-linear problems*, Tech. Rep. 2/2005, Norwegian University of Science and Technology, 2005.
- [40] S. P. NØRSETT, *An A-stable modification of the Adams-Bashforth methods*, in Conference on the numerical solution of differential equations (Dundee, 1969), Springer, Berlin, 1969, pp. 214–219.
- [41] A. OSTERMANN, M. THALHAMMER, AND W. M. WRIGHT, *A class of explicit exponential general linear methods*, BIT, 46 (2006), pp. 409–431.
- [42] D. A. POPE, *An exponential method of numerical integration of ordinary differential equations*, Communications of the ACM, 6 (1963), pp. 491–493.
- [43] G. RAINWATER AND M. TOKMAN, *A new class of split exponential propagation iterative methods of Runge-Kutta type (sEPIRK) for semilinear systems of ODEs*, J. Comput. Phys., 269 (2014), pp. 40–60.
- [44] ———, *A new approach to constructing efficient stiffly accurate EPIRK methods*, submitted, (2015).
- [45] H. H. ROSENBRock, *Some general implicit processes for the numerical solution of differential equations*, Computer, 5 (1963), pp. 329–330.
- [46] J. SCHNAKENBERG, *Simple chemical reaction systems with limit cycle behaviour*, J. theor. Biol., 81 (1979), pp. 389–400.
- [47] G. I. SIVASHINSKY, *Nonlinear analysis of hydrodynamic instability in laminar flames—i. Derivation of basic equations*, Acta Astronautica, 4 (1977), pp. 1177–1206.
- [48] K. STEWARTSON AND J. T. STUART, *A non-linear instability theory for a wave system in plane Poiseuille flow*, J. Fluid Mech., 48 (1971), pp. 529–545.
- [49] P. SUBRAMANIAN, A. J. ARCHER, E. KNOBLOCH, AND A. M. RUCKLIDGE, *Three-dimensional phase field quasicrystals*, submitted.
- [50] J. SWIFT AND P. C. HOHENBERG, *Hydrodynamic fluctuations at the convective instability*, Phys. Rev. A, 15 (1977), pp. 319–328.
- [51] M. TOKMAN, *Efficient integration of large stiff systems of ODEs with exponential propagation iterative (EPI) methods*, J. Comput. Phys., 213 (2006), pp. 748–776.
- [52] ———, *A new class of exponential propagation iterative methods of Runge-Kutta type (EPIRK)*, J. Comput. Phys., 230 (2011), pp. 8762–8778.
- [53] M. TOKMAN AND J. LOFFELD, *Efficient design of exponential-Krylov integrators for large scale computing*, Procedia Comp. Sci., 1 (2012), pp. 229–237.
- [54] M. TOKMAN, J. LOFFELD, AND P. TRANQUILLI, *New adaptive exponential propagation iterative methods of Runge-Kutta type*, SIAM J. Sci. Comput., 34 (2012), pp. A2650–A2669.
- [55] A. TOWNSEND AND L. N. TREFETHEN, *An extension of Chebfun to two dimensions*, SIAM J. Sci. Comput., 35 (2013), pp. C495–C518.
- [56] A. TOWNSEND, H. WILBER, AND G. B. WRIGHT, *Computing with functions in spherical and polar geometries, I. The sphere*, SIAM J. Sci. Comput., submitted.
- [57] L. N. TREFETHEN, *Spectral Methods in MATLAB*, SIAM, Philadelphia, 2000.
- [58] L. N. TREFETHEN AND J. A. C. WEIDEMAN, *The exponentially convergent trapezoidal rule*, SIAM Rev., 56 (2014), pp. 385–458.
- [59] A. M. TURING, *The chemical basis of morphogenesis*, Phil. Trans. Roy. Soc. Lon. (Ser. B), 237 (1952), pp. 37–72.
- [60] P. J. VAN DER HOUWEN, *Construction of integration formulas for initial value problems*, North-Holland Publishing Co., Amsterdam, 1977.
- [61] G. B. WRIGHT, M. JAVED, H. MONTANELLI, AND L. N. TREFETHEN, *Extension of Chebfun to periodic functions*, SIAM J. Sci. Comput., 37 (2015), pp. C554–C573.